Synthesis, Crystal Structure, Thermal, Magnetic Properties and DFT Computations of a Ytterbium(III) Complex Derived from Pyridine-2,6-Dicarboxylic Acid

Shahzad Sharif (mssharif@gcu.edu.pk)
Govt College University, Lahore https://orcid.org/0000-0001-5400-1154
Maham Saeed
GC University
Necmi Dege
Ondokuz Mayıs University
Rehana Bano
University of the Punjab
Mazhar Amjad Gilani
COMSATS University Islamabad
Onur Sahin
Sinop University
Saeed Ahmad
Prince Sattam bin Abdulaziz University
Ayoub Rashid Ch
GC University

Research Article

Keywords: Ytterbium(III), Pyridine-2,6-dicarboxylic acid, X-ray structure, magnetic properties, DFT computation

Posted Date: November 2nd, 2021

DOI: https://doi.org/10.21203/rs.3.rs-1010687/v1

Abstract

A new ytterbium(III) complex, $(DMAH_2)_3[Yb(Pydc)_3].4H_2O$ **(1)** {Pydc = Pyridine-2,6-dicarboxylate anion, DMAH = Dimethylamine} has been prepared under mild solvothermal conditions and characterized by elemental analysis, IR spectroscopy, thermal analysis and single crystal X-ray diffraction. The DMAH molecules in **1**, generated in situ from hydrolysis of *N*,*N*-dimethylformamide are responsible to assemble 2D coordination polymers through N-H•••O and O-H•••O hydrogen bonding. Magnetic susceptibility measurements indicate that the complex (**1**) obeys the Curie Weiss law and the overall magnetic behavior is typical for the presence of weak antiferromagnetic exchange coupling interactions. Theoretical data for geometrical parameters of complex **1** agree well with the experimental data. Large HOMO-LUMO energy gap of 4.33 eV has provided kinetic stability to the complex **1**. NBO analysis reflects that intramolecular charge transfer occurred between ligand and metal orbitals with the highest stabilization energy of 1024.04 kcal/mol. The negative electrostatic potential at the nitrogen and dianionic pyridine-2,6-dicarboxylate regions confirms that these are dynamic locations for Yb(III) binding.

1. Introduction

Due to its rigidity and high symmetry, pyridine-2,6-dicarboxylic acid (H_2Pydc) is a typical ligand for constructing lanthanide coordination polymers [1–12]. It can adopt varied coordination modes such as monodentate, chelating bidentate, bridging bidentate and multidentate. The carboxylate groups on the pyridine ring can be fully or partially deprotonated for coordination to metals. The carboxylic O atoms are also beneficial to form hydrogen bonds, while the rigid pyridyl ring is a general origin of π-π stacking interactions. The diverse coordination patterns of N or O atoms can result in formation of discrete or infinite structures as evidenced by the crystal structures of several H_2Pydc-based lanthanide complexes [1–12].

Lanthanide compounds based on Pyridine-2,6-dicarboxylic acid (H_2Pydc) have attracted extensive attention in florescence materials due to their diverse applications, such as sensing materials, lighting and bio-medical imaging devices [1]. Lanthanide compounds with visible light emission mostly concentrate on Sm(III), Eu(III), Tb(III) and Dy(III) [5, 12–14], while the compounds containing Er(III) exhibit NIR luminescence [15]. Zhao and co-workers have reported a variety of lanthanide compounds with H_2Pydc, which include 4f, 4f-2p, 4f-3d and 4f-4d systems, and reveal the relationship between the structures and luminescent properties [1, 16–19]. The luminescent investigations indicate that H_2pydc ligand can act as an antenna to stimulate the photosensitization of lanthanides.

Considering the possible role of lanthanide complexes for material applications, we have earlier reported the crystal structures of several lanthanide complexes with pyridine-2,6-dicarboxylic acid (H_2Pydc) ligand [9, 20–23]. In these complexes the lanthanide atoms exhibit a nine-coordination environment, while H_2Pydc coordinates in neutral, monoanionic and dianionic forms. To further explore the coordination chemistry of lanthanide-Pydc complexes to generate supramolecular networks through H-bonding. We

report here the synthesis, structural characterization, thermal and magnetic properties as well as comprehensive DFT computations of a new anionic ytterbium(III) complex stabilized by dimethylammonium ions.

2. Experimental

2.1 Materials and Measurements

All reagents were purchased commercially and were used without further purification. The percentage detection of H, C and N was performed on the Elemental Analyzer, Vario Micro Cube, Elementar, Germany. IR spectra were recorded on Perkin-Elmer FT-IR 180 spectrophotometer using KBr pellets over the range of 4000–400 cm^{-1}. Thermal analysis (25-1000°C) was performed under continuous nitrogen flow, with a ramp-rate of 10 °C min^{-1} using a SDT Q600 instrument (TA Instruments, USA). The temperature dependence magnetic susceptibility measurements were made in the temperature range of 5-300 K using Superconducting Quantum Interference Device (SQUID-MPMS-5, USA) at an applied magnetic field of 1000Oe. The results are shown as plots of χ_m, χ_m^{-1} and $\chi_m T$ *versus* T (χ_m = molar magnetic susceptibility) using Origin software [24]. The effective magnetic moment, μ_{eff}, were calculated by applying the relation $\mu_{eff} = 2.828\ (\chi_m T)^{1/2}$ in Bohr magneton (μ_B) [25, 26].

2.2 Synthesis of $(DMAH_2)_3[Yb(Pydc)_3].4H_2O$ (1)

A mixture of H_2Pydc (84 mg, 0.50 mmol), 6 mL of water and 3 mL of DMF was stirred at 90°C for half an hour followed by drop-wise addition of 5 mL aqueous solution of ytterbium chloride hexahydrate ($YbCl_3.6H_2O$; 136 mg, 0.35 mmol). The mixture was refluxed for four hours along with stirring to obtain a clear solution, Off-white block-like crystals slowly grew in the filtered solution as solvent evaporated over one month and recovered by filtration, rinsed with mixture of water and DMF, and dried at room temperature. Analysis (%) Calc. for $C_{27}H_{41}N_6O_{16}Yb$ (878.70): N, 9.56; C, 36.87; H, 4.67; Found: N, 9.42; C, 37.07; H, 4.71. Yield *ca.* 50 %. IR (cm^{-1}): 3419–3253 v(O–H, N–H) broad, strong); 1607 v_{asym}(C=O); 1447 v_{sym}(C=O); 1560 v_{asym}(–NH_2).

2.3 X-ray Structure Determination

Suitable crystals of complex **1** were selected for data collection, which was performed on a Bruker KAPA APEX II CCD diffractometer equipped with a graphite-monochromatic Mo-K_α radiation at 296 K. The structure was solved by direct methods using SHELXS-97 and CRYSTALS [27, 28], and refined by full-matrix least-squares methods on F^2 using SHELXL-97 and CRYSTALS [27, 28] within the WINGX [29] suite of software. All non-hydrogen atoms were refined with anisotropic parameters. Water H atoms were located in a difference map and refined subject to a DFIX restraint of O-H = 0.83(2) Å. All other H atoms were located from different maps and then treated as riding atoms with C-H distances of 0.93-0.96Å and N-H distances of 0.90Å. Molecular diagrams were created using MERCURY [30]. Supramolecular analyses

were made and the diagrams were prepared with the aid of PLATON and CrystalMaker® [31, 32]. Details of data collection and crystal structure determinations are given in Table 1.

Table 1
Crystal data and structure refinement parameters for **1**.

Empirical formula	$C_{27}H_{41}N_6O_{16}Yb$
Formula weight	878.70
Crystal system	Monoclinic
Space group	$P2_1/c$
a (Å)	9.8111 (4)
b (Å)	20.5590 (8)
c (Å)	18.1876 (6)
β (º)	109.608 (2)
V (Å^3)	3455.8 (2)
Z	4
D_c (g cm^{-3})	1.689
μ (mm^{-1})	2.79
θ range (º)	1.6-28.3
Measuredrefls.	31391
Independent refls.	8568
R_{int}	0.030
S	1.18
R1/wR2	0.027/0.078
$\Delta\rho_{max}/\Delta\rho_{min}$ (eÅ^{-3})	0.67/−0.93

Computational studies

All the DFT calculations of synthesized complex **1** are performed by using Gaussian 16 program Package [33] and are visualized by using GaussView 6.1.1 software [34]. Geometry optimization of complex **1** is carried out at B3LYP/SDD and M06-2X/SDD levels of theory to compare results of both methods with experimental data. Frequency calculations are also performed at the respective levels of theory to assure

local minima. The B3LYP/SDD level of theory is most reliable and has been widely used for the ytterbium complexes [35]. The B3LYP/SDD employs three-parameter Becke (B3) exchange functional [36], Lee-Yang-Parr (LYP) nonlocal correctional functional [37], and Stuttgart SDD basis set [38]. Frontier molecular orbital (FMO) analysis, reactivity parameters, natural bond orbital (NBO) analysis and molecular electrostatic potential (MEP) analysis of complex **1** are also performed at the same level of theory. Visualization of FMOs and MEP surface is carried out by using Multiwfn [39] and VMD [40] softwares. Furthermore, Hirshfeld surface analysis of complex **1** is performed by using Crystal Explorer software [41].

3. Results And Discussion

3.1 IR and Thermal Studies

The reactions of $YbCl_3.6H_2O$; with H_2Pydc in a 1:1 molar ratio in a mixture of water and DMF under solvothermal conditions resulted in formation of a crystalline complex, $(DMAH_2)_3[Yb(Pydc)_3].4H_2O$ **(1)**. The DMAH molecules in **1** were generated in situ from hydrolysis of *N*,*N*-dimethylformamide [21]. In the IR spectrum of complex **1**, a broad peak in the region of 3419–3253 cm^{-1} was observed, which was assigned to the O–H and N–H stretching vibrations of water molecules and dimethylaminium ions respectively. The band at 1560 cm^{-1} is related to the N-H bending vibration of dimethylaminium ions. The characteristic absorptions for the asymmetric and symmetric stretches of carboxylate group are found at 1607 and 1447 cm^{-1} respectively, while in the IR spectrum of free ligand, these bands are observed at 1688 and 1375 cm^{-1} respectively. A significant shift of the asymmetric mode, $v_{as}(COO)$ towards the lower wavenumber upon coordination and that of the symmetric mode, $v_s(COO)$ towards the higher wavenumber indicates the binding of Pydc ligand to the metal through the carboxylate oxygen atoms [20].

The thermal decomposition of complex **1** is illustrated in Figure 1. At the first stage four non-coordinated water molecules are released at 90°C corresponding to the weight loss of 9.3 % (calculated 8.2 %). The loss of water is associated with an endothermic transition in DSC. The next weight loss of 39 % between 210°C and 350°C corresponds to the removal of two Pydc ligands (calculated 37.6 %). The difference indicates the removal of some other volatile component like ammonia or dimethylamine.The DSC curve exhibits an endothermic transition at 305 ^oC. The elimination of the third Pydc ligand takes place after 500°C (19.5 % wt loss against the theoretical value of 18.8 %) and is marked by an exothermic transition in DSC at 520°C. Beyond this point the remaining organic moieties are lost up to 950°C leaving behind a residue of 24 %, which is attributed to Yb_2O_3 (calcd. 22.5%). The thermal data agrees well the results obtained from the elemental analysis.

3.2 Crystal structure of Complex 1

The molecular structure of complex **1**, $(DMAH_2)_3[Yb(Pydc)_3].4H_2O$ with the atom labeling is shown in Figure 2. The selected bond lengths and angles are given in Table S1. The complex **1** exists as a monomeric ionic species consisting of an ionic complex $[Yb(Pydc)_3]^{3-}$, three dimethylammonium counter ions and four non-coordinated water molecules (Figure 2). The DMAH molecules are generated *in situ* from hydrolysis of *N,N*-dimethylformamide [21]. The Yb(III) ion in **1** is coordinated by three dianionic pyridine-2,6-dicarboxylate ligands ($Pydc^{2-}$) and attains a distorted tricapped trigonal prismatic YbN_3O_6 coordination geometry with the N atoms serving as the caps protruding through the prismatic side-faces (Figure S1). The N-Yb-N bond angles are closer to 120° (116.28(8)°-122.72(9)°), while the O-Yb-O bond angles ranged between 74.94(8)°-146.01(8)°. The distortion in tricapped trigonal prismatic geometry is attributed to the upper and lower distorted triangular faces with mean deviations of -1.802º and 6.426º from regular triangular faces respectively. Of the 14 triangular faces of YbN_3O_6 polyhedron, the dihedral angles between O3-O9-N3 and O9-O7-N2 faces are 59.902º and 63.507º, while between the relatively distorted triangular faces O5-O11-N3 and O5-O1-N2, they are 52.435º and 54.713º. The dihedral angles between N3-N2-N1, N2-N1-N3 and N1-N3-N2 triangular faces are 61.161º, 60.468º and 58.372º respectively. The Yb-N and Yb-O bond lengths fall in the ranges, 2.361(2)Å-2.386(2) Å and 2.440(2)-2.461(3) Å, respectively. These data are in agreement with the corresponding values of the similar reported Yb(III) complexes [42–45]. The pyridine ring mean planes are approximately planar, with the maximum deviations of 0.0102(22) Å for C(5) atom (C(8) and C(16) atoms are deviated by 0.0066(25) Å and 0.0052(26) Å respectively). The structural features of **1** are closely related to the other $[Ln(Pydc)_3]^{3-}$ type complexes [6, 11, 21, 23].

We have earlier reported the crystal structures of a similar series of the Pydc-based coordination polymers with the formula $[Ln(Pydc)_3](DMAH_2).H(DMAH)_2$ (Ln = Ce, Ho, Nd, Sm) [21]. Their structural analysis reveals that their metal coordination sphere is quite identical to that of compound **1**. Pydc ligand in these complexes as well as in **1** adopts only one kind of coordination modes, where the oxygen atoms of the carboxylate groups and the nitrogen atom of a pyridine ring form a chelate with the metal atom.

Within the structure of **1**, extensive hydrogen-bonding interactions take place between the carboxylate groups, water molecules and ammonium ions. The molecules of **1** are linked to each other by a combination of N-H•••O, O-H•••O and C-H•••O hydrogen bonds (Table S2). The amnonium nitrogen atom N(5) in the molecule at (x, y, z) acts as hydrogen-bond donor, *via* atoms H(5A) and H(5B), to carboxylate oxygen atoms $O(6)^{ii}$ and O(7), forming a $C_2^2(8)$ chain running parallel to the [100] direction. The water oxygen atom O(14) in the reference molecule at (x, y, z) acts as hydrogen-bond donor, *via* atoms H(14A) and H(14B), to atoms $O(4)^{v}$ and $O(12)^{vi}$, forming a $C_2^2(10)$ chain running parallel to the [100] direction. Similarly, the carboxylate atoms O(6) and $O(8)^{vii}$ accept hydrogen bonds from H(16A) and H(16B) of water atom O(16) yielding a $C_2^2(10)$ chain running parallel to the [100] direction. Finally, dimethylamine and water molecules link neighboring polymeric chains *via* N-H•••O and O-H•••O hydrogen bonds into a two-dimensional framework parallel to the *ac* plane (Figure S2).

3.3 Magnetic Measurement

The magnetic behavior of complex **1** is represented in the forms of χ_m, χ_m^{-1} *and* $\chi_m T$ *vs.* T plots (χ_m = molar magnetic susceptibility) shown in Figure S3. The susceptibility can be well described by the Curie–Weiss law above 40 K with a Curie constant C = 3.11 ± 0.0022 $cm^3K\ mol^{-1}$ and Weiss constant θ = –35.52 K. In the high temperature end (300 K), $\chi_m T$ = 2.69 $cm^3K\ mol^{-1}$ provides an effective magnetic moment μ_{eff} of 4.64 μ_B, which is slightly larger than the expected multiplet $^2F_{7/2}$ value of 4.50 μ_B per formula for one Yb(III) ion of one uncoupled (g_J = 1.1) Yb(III) ion [46]. The product of $\chi_m T$ was found to decrease with decreasing temperature to reach a final value of 0.97 cm^3Kmol^{-1} at 5 K with an effective magnetic moment of 2.79 μ_B. The overall behavior of $\chi_m T$ with temperature and the negative value of θ is typical for the presence of weak antiferromagnetic exchange coupling interactions.

3.4. DFT computations

3.4.1 Geometrical parameters

Molecular geometry of complex **1** is optimized by taking its X-ray crystallographic CIF file. The results of geometrical parameters obtained at two different methods B3LYP and M06-2X are compared with experimental data and are listed in Table 2.

Table 2
Experimental and theoretical bond lengths (Å) and bond angles (degree) of Complex **1**

Complex 1 Bond Lengths							
Bond Length	Experimental	Theoretical		Bond Length	Experimental	Theoretical	
		B3LYP	M06-2X			B3LYP	M06-2X
N1-Yb1	2.453	2.471	2.432	O7-Yb1	2.361	2.394	2.357
O1-Yb1	2.371	2.326	2.297	N3-Yb1	2.441	2.483	2.454
O3-Yb1	2.386	2.406	2.386	O9-Yb1	2.368	2.412	2.339
N2-Yb1	2.461	2.471	2.451	O11-Yb1	2.362	2.348	2.321
O5-Yb1	2.365	2.323	2.324				
Complex 1 Bond Angles							
Bond Angle	Experimental	B3LYP	M06-2X	Bond Angle	Experimental	B3LYP	M06-2X
O5-Yb1-O9	88.52	88.12	84.65	N3-Yb1-N2	120.99	120.58	123.21
O11-Yb1-O3	83.92	92.35	94.55	O9-Yb1-O3	80.39	73.01	72.15
N1-Yb1-N2	116.28	122.08	124.06	O5-Yb1-N3	73.63	70.89	71.43
O7-Yb1-O1	88.24	90.45	91.07	N3-Yb1-N1	122.72	117.32	112.72
O11-Yb1-N1	73.06	69.88	68.61				

The results clearly depict that the bond lengths and bond angles computed at B3LYP method are in good agreement with the experimental data than M06-2X method. The theoretical bond lengths at B3LYP/SDD for N1-Yb1, O3-Yb1, N2-Yb1 and O11-Yb1 b match well with the experimental data and are 2.471 Å (Exp. 2.453 Å), 2.406 Å (Exp. 2.386 Å), 2.471 Å (Exp. 2.461 Å) and 2.348 Å (Exp. 2.362 Å). However, there is minor deviation less than 1 Å in some bond lengths between theoretical and experimental X-ray crystallographic data. The highest deviation (0.045 Å) in theoretical bond length is observed for O1-Yb1 bond from the experimental one. Similarly, the theoretical bond angles that correlate better with the experimental data are O5-Yb1-O9, O7-Yb1-O1, N3-Yb1-N2, and O5-Yb1-N3 and their values are 88.12° (Exp. 88.52°), 90.45° (Exp. 88.24°), 120.58° (Exp. 120.99°) and 70.89° (Exp. 73.63°). Some theoretical bond angles are bigger than the experimental ones such as O11-Yb1-O3 (92.35°) and N1-Yb1-N2 (122.08°). The reason behind the fact is that DFT calculations are performed in gas phase while experimental data is obtained in solid phase. The optimized structure of complex **1** is displayed in Figure 3.

3.4.2 Frontier molecular orbital analysis

Electronic characteristics and reactivity of any complex can be estimated via frontier molecular orbital analysis. Molecular orbital energies are computed at the B3LYP method along with SDD basis set and pictorial representation of HOMO (highest occupied molecular orbital) and LUMO (lowest unoccupied molecular orbital) electron densities along their energy gap is provided in Figure 4. The electron density of HOMO is localized at the carboxylate group of dianionic pyridine-2,6-dicarboxylate ligand ($Pydc^{2-}$) while the LUMO orbital electron density is localized at the pyridinic moiety of complex **1**. Energies of HOMO and LUMO are -6.12 eV and -1.78 eV, respectively. Complex **1** has a 4.33 eV HOMO-LUMO energy gap (Eg) indicating that it has excellent kinetic stability and low chemical reactivity.

Some reactivity parameters including ionization potential (I), electron affinity (A), chemical potential (μ), chemical hardness (η), chemical softness (S) and electrophilicity index (ω) are also calculated for the complex **1** and listed in Table 3. The chemical potential of -3.95 eV shows that the complex **1** is thermodynamically stable. It is an essential parameter for calculation of other electronic parameters. A larger chemical hardness value (2.16 eV) than that of chemical softness (1.08 eV) reflects that the complex **1** is thermodynamically stable and less reactive. A lower electrophilicity index (ω) value of complex **1** supports its nucleophilic nature.

Table 3
HOMO, LUMO energies, energy gap E_g (eV) and their quantum reactivity parameters

Parameter	Energies (au)	Energies (eV)
HOMO	-0.22472	-6.12
LUMO	-0.06576	-1.78
E_g	0.15901	4.33
I	0.22472	6.12
A	0.06576	1.78
μ	-0.14524	-3.95
η	0.07948	2.16
S	0.03974	1.08
ω	0.132704	3.62

Other thermodynamic parameters of complex **1** have been computed theoretically to confirm the chemical stability. Total energy, heat capacity at constant volume, entropy and zero point vibrational

energy of complex **1** are 483.38 kcal/mol, 206.43 cal/mol-kelvin, 332.109 cal/mol-kelvin and 446.67 kcal/mol. Similarly, rotational constants are also computed for complex **1** and are listed in Table S3.

3.4.3 Natural bond orbital (NBO) analysis

NBO analysis of the complex **1** is performed at the B3LYP/SDD level of theory by using built-in Gaussian NBO Version 3.1. Natural bond orbital analysis provides a valuable understanding of the intermolecular and intra-molecular interactions, hydrogen bonding and charge transfer between atoms of any molecular structure [47, 48]. It also depicts electrical charge displacement and conjugative interactions. The loss of occupancy from a localized NBO (donor) of Lewis structure to an empty non-Lewis NBO (acceptor) causes interactions. Second order perturbation theory analysis of Fock matrix has been carried out to observe the donor-acceptor NBO transitions for complex **1**. The stabilization energy for donor (i) to acceptor (j) delocalization can be calculated as follows:

$$E^{(2)} = q_i \frac{F^2(i,j)}{\epsilon_j - \epsilon_i}(1)$$

Where q_i is occupancy of donor orbital, ε_j, ε_i are diagonal elements and F (i,j) is off-diagonal Fock matrix element. Larger value of stabilization energy $E^{(2)}$ between electron donor and acceptor orbitals increases the stability of the synthesized complex. Some major donor to acceptor NBO transitions starting from the highest $E^{(2)}$ are listed in Table S4.

These results reflect that many NBO transitions have occurred between different energy levels of complex **1**. The highest stabilization energy value of 1024.04 kcal/mol is observed from O_{89}-H_{91} donor to antibonding O_{80}-H_{82} acceptor orbital. The second largest $E^{(2)}$ of 606.13 kcal/mol is obtained by the charge transfer from lone pair of O_{89} to antibonding O_{80}-H_{82} orbital and so on. These stronger intramolecular interactions with larger stabilization energies might be responsible for the stability of complex **1**.

3.4.4 Molecular electrostatic potential (MEP) analysis

Molecular electrostatic potential analysis is the best tool to analyze the charge distribution of a molecular structure [49]. The electrophilic and nucleophilic sites in a molecule are described by MEP which is associated with electron density. In complex **1**, more prominent red color patches at dianionic pyridine-2,6-dicarboxylate portion reflect the nucleophilic region with more negative potential. The blue color patches at dimethylammonium ions show the electrophilic nature. The molecular electrostatic potential surface of complex **1** is shown in Figure 5.

3.4.5 Hirshfeld surface analysis

Hirshfeld surface analysis is a useful tool for describing the space occupied by molecules in a crystal for partitioning of crystals electron density into molecular fragments [50]. It has a key contribution in defining

the surface properties of molecules and provides information more about the intermolecular interactions of molecular crystals. Hirshfeld surface investigations of complex **1** is performed by using Crystal Explorer program from the X-ray crystallographic CIF file. Intermolecular interactions of complex **1** are best quantified by using Hirshfeld surfaces and their corresponding two-dimensional fingerprint plots. The d_{norm} mapped surface of complex **1** is shown in Figure 6.

The red patches in the surface map of complex **1** correspond to the hydrogen bonding between O-H···O and C-H···O atoms. The white regions indicate weak van der Waals interaction and blue patches covering a large area are for the longer than van der Waals interactions. Furthermore, 2D fingerprint plots for the intermolecular percentage contribution of atom to atom in complex **1** is shown in Figure S4. The results show that the highest intermolecular percentage contribution for complex **1** is from H···H atom up to 45.5%. The %age contributions from O···H and H···O atoms are 20.7% and 18%, respectively. Similarly, intermolecular %age contributions of C···H and H···C atoms are 6.4% and 5.6% and so on.

4 Conclusions

In this paper, a new zero dimensional ytterbium(III) complex with Pydc ligand has been synthesized under mild solvothermal condition. Extensive N-H···O and O-H···O bonding due to dimethylamine and water molecules are responsible for two two-dimensional framework. Solvent molecules and in situ generation of molecules like dimethylamine can be tuned for preferred structural topologies and cross-linking in to 2D and 3D coordination networks. Density functional theory simulations have been carried out for computing the geometrical parameters of complex 1 and the results are compared with the experimental data for reliability. Larger values of HOMO-LUMO energy gap (4.33 eV) and chemical hardness (2.16 eV) reflected that the complex is stable and less reactive in nature. NBO analysis has provided information about the nature of interactions and intermolecular charge transfer transitions from donor to acceptor orbitals. MEP analysis of complex 1 reveals that more electron density with negative electrostatic potential at the nitrogen and dianionic pyridine-2,6-dicarboxylate regions is responsible for ligand strong bonding with Yb(III) metal. Furthermore, dnorm Hirshfeld surface map indicates the nature of intermolecular interactions of molecular crystal. Its 2D fingerprint plots have the highest %age contribution of molecular surface from H…H (45.5%) followed by O…H (20.7%).

Declarations

Acknowledgement

We gratefully acknowledge financial assistance from the Higher Education Commission of Pakistan, HEC project no. 01-ISULL/09/GCUL/ACAD/HEC/2017/166 and Office of Research Innovation & Commercialization GC University, Lahore, ORIC project no. 108/ORIC/19.

References

1. Xiang, D.-X. Bao, J. Wang, J., Y.-C. Li, X.-Q. Zhao, J. Lumin. **186**, 273-282 (2017)
2. -L. Gao, L. Yi, B. Zhao, X.-Q. Zhao, P. Cheng, D.-Z. Liao, S.-P. Yan, Inorg. Chem. **45**, 5980–5988 (2006)
3. K. Prasad, M.V. Rajasekharan, Inorg. Chem.48, 11543–11550 (2009)
4. Ay, E. Yildiz, I. Kani, Polyhedron. **142**, 1-8 (2018)
5. Zhu, K. Ikarashi, T. Ishigaki, K. Uematsu, K. Toda, H. Okawa, M. Sato, Inorg. Chim. Act. **362**, 3407-3414 (2009)
6. A. Brayshaw, A.K. Hall, W.T.A. Harrison, J.M. Harrowfield, D. Pearce, T.M. Shand, B.W. Skelton, C.R. Whitaker, A.H. White, Eur. J. Inorg. Chem. 1127-1141 (2005)
7. Zhao, L. Yi, Y. Dai, X.Y. Chen, P. Cheng, D.Z. Liao, S.P. Yan, Z.H. Jiang, Inorg. Chem. **44**, 911-920 (2005)
8. Chuasaard, K. Panyarat, P. Rodlamul, K. Chainok, S. Yimklan and A. Rujiwatra, Cryst. Growth Des. **17**, 1045-1054 (2017)
9. Sharif, I.U. Khan, O. Şahin, S. Ahmad, O. Buyukgungor, S. Ali, J. Inorg. Organomet. Polym. Mater. **22**, 1165-1173 (2012)
10. -Z. Du, Y.-Y. Wang, Y.-Y. Xie, H.-T. Li, T.-F. Liu, J. Mol. Struct. **1108**, 96 (2016)
11. Hojnik, M. Kristl, A. Golobic, A. Golobic, Z. Jaglicic, M. Drofenik, J. Mol. Struct. **1079**, 54-60 (2015)
12. G. Huang, D.Q. Yuan, Y.Q. Gong, F.L. Jiang, M.C. Hong, J. Mol. Struct. **872**, 99–104 (2008)
13. M. Chen, Q. Gao, D. Gao, D. Wang, Y. Li, W. Liu, W. Li, J. Coord. Chem. **66**, 3829–3838 (2013)
14. Chen, W. Chen, Z. Ju, Q. Gao, T. Lei, W. Liu, Y.H. Li, D.D. Gao, W. Li, Dalton Trans. **42**, 10495–10502 (2013)
15. Feng, J.-S. Zhao, L.-Y. Wang, X.-G. Shi, Inorg. Chem. Commun. **12**, 388–391 (2009)
16. Zhao, X.-Q. Zhao, Z. Chen, W. Shi, P. Cheng, S.-P. Yan, D.-Z. Liao, CrystEngComm. **10**, 1144–1146 (2008)
17. -Q. Zhao, Y. Zuo, D.-L. Gao, B. Zhao, W. Shi, P. Cheng, Cryst. Growth Des. **9**, 3948–3957 (2009)
18. -Q. Zhao, B. Zhao, W. Shi, P. Cheng, CrystEngComm. **11**, 1261–1269 (2009)
19. -Q. Zhao, P. Cui, B. Zhao, W. Shi, P. Cheng, DaltonTrans. **40**, 805–819 (2011)
20. Sharif, O. Şahin, B. Khan, I.U. Khan, J. Coord. Chem. **68**, 2725-2738 (2015)
21. Sharif, B. Khan, O. Şahin, I.U. Khan, Russ. J. Coord. Chem. **42**, 56-65 (2016)
22. Sharif, I.U. Khan, O. Sahin, N. Jabeen, S. Ahmad, B. Khan, Z. Naturforsch. B. **74**, 255-260 (2019)
23. Sharif, S. Zaheer, M.W. Mumtaz, O. Sahin, S. Ahmad, S. Zulfiqar, A. Adnan, I.U. Khan, Russ. J. Coord. Chem. **47**, 95-104 (2021)
24. OriginPro 8 SRO, V 8.0724 (B724), Northampton MA 01060, USA. (originLab.com).
25. Blundell, D. Thouless, Magnetism in condensed matter, Oxford University Press: U.K., **29** (2001)
26. Want, F. Ahmad, P.N. Kotru. J. Alloys Comp. **448**, L5-L6 (2008)
27. M. Sheldrick, Acta Cryst. A**64**, 112-122 (2008)

28. W. Betteridge, J.R. Carruthers, R.I. Cooper, K. Prout, D.J. Watkin. J. Appl. Cryst. **36**, 1487 (2003)
29. J. Farrugia, J. Apply. Cryst. **32**, 837-838 (1999)
30. F. Macrae, I.J. Bruno, J.A. Chisholm, P.R. Edgington, P. McCabe, E. Pidcock, P.A. Wood, J. Appl. Cryst. **41**, 466-470 (2008)
31. L. Spek, J. Appl. Crystallogr. **26**, 1-7 (2003)
32. Crystal and molecular structures program for Mac and Windows. CrystalMaker® software, Ltd, Oxford, England (crystalmaker.com).
33. J. Frisch, G.W. Trucks, H.B. Schlegel, G.E. Scuseria, M.A. Robb, J.R. Cheeseman, G. Scalmani, V. Barone, G.A. Petersson, H. Nakatsuji, X. Li, M. Caricato, A.V. Marenich, J. Bloino, B.G. Janesko, R. Gomperts, B. Mennucci, H.P. Hratchian, J.V. Ortiz, A.F. Izmaylov, J.L. Sonnenberg, D. Williams-Young, F. Ding, F. Lipparini, F. Egidi, J. Goings, B. Peng, A. Petrone, T. Henderson, D. Ranasinghe, V.G. Zakrzewski, J. Gao, N. Rega, G. Zheng, W. Liang, M. Hada, M. Ehara, K. Toyota, R. Fukuda, J. Hasegawa, M. Ishida, T. Nakajima, Y. Honda, O. Kitao, H. Nakai, T. Vreven, K. Throssell, J.A. Montgomery, Jr, J.E. Peralta, F. Ogliaro, M.J. Bearpark, J.J. Heyd, E.N. Brothers, K.N. Kudin, V.N. Staroverov, T.A. Keith, R. Kobayashi, J. Normand, K. Raghavachari, A.P. Rendell, J.C. Burant, S.S. Iyengar, J. Tomasi, M. Cossi, J.M. Millam, M. Klene, C. Adamo, R. Cammi, J.W. Ochterski, R.L. Martin, K. Morokuma, O. Farkas, J.B. Foresman, and D.J. Fox, Gaussian 16, revision B. 01, Gaussian, Inc.,Wallingford CT, (2016)
34. GaussView, Version 6.1.1, Roy Dennington, Todd Keith, and John Millam, Semichem Inc., Shawnee Mission, KS, 2019.
35. Paswan, A. Anjum, N. Yadav, N. Jaiswal, R.K.P. Singh, J. Coord. Chem. **73**, 686-701 (2020)
36. D. Becke, Int. J. Quantum Chem. **36**, 599-609. (1989)
37. Lee, W. Yang, R.G. Parr, Phys. Rev. B. **37**, 785 (1988)
38. Andrae, U. Haeussermann, M. Dolg, H. Stoll, H. Preuss, Theor. Chim. Acta,**77**, 123-141 (1990)
39. Lu, F. Chen, J. Comput. Chem. **33**, 580-592 (2012)
40. Humphrey, A. Dalke, K. Schulten, J. Mol. Graph. **14**, 33-38 (1996)
41. R. Spackman, M.J. Turner, J.J. McKinnon, S.K. Wolff, D.J. Grimwood, D. Jayatilaka, M.A. Spackman, J. App. Crystallogr. **54** (2021)
42. Hojnik, M. Kristl, A. Golobic, Z. Jaglicic, M. Drofenik, Cent. Eur. J. Chem. **12**, 220-226 (2014)
43. Hussain, I.U. Khan, M. Akkurt, S. Ahmad, M.N. Tahir, Russ. J. Coord. Chem. **40**, 686-694 (2014)
44. -B. Bo, G.-X. Sun, D.-L.Geng, Inorg. Chem. **49**, 561–571 (2009)
45. G. Reddy, N. Mamidi, C.P. Pradeep, CrystEngComm. 18, 4272-4276 (2016)
46. D. L. Carlin, Magnetochemistry, Springer Verlag, Berlin, (1986)
47. E. Reed, F. Weinhold, J. Chem. Phys. **78**, 4066-4073 (1983)
48. E. Reed, F. Weinhold, J. Chem. Phys. **83**, 1736-1740 (1985)
49. S. Murray, P. Politzer, Wiley Interdiscip. Rev. Comput. Mol. Sci. **1**, 153-163 (2011)

50. M.A. Spackman, D. Jayatilaka, CrystEngComm, **11**, 19-32 (2009)

Figures

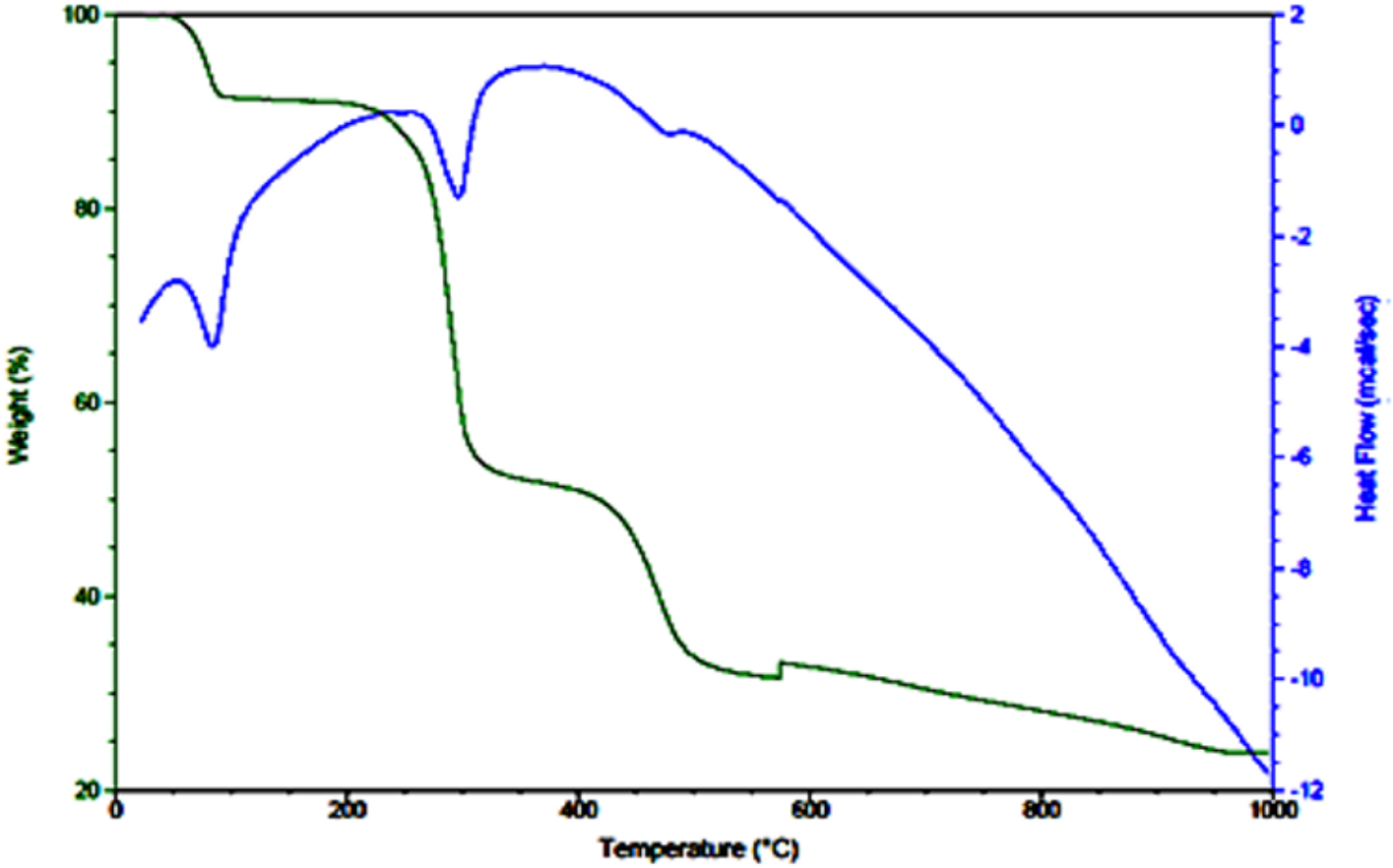

Figure 1

TGA/DSC Curve of 1

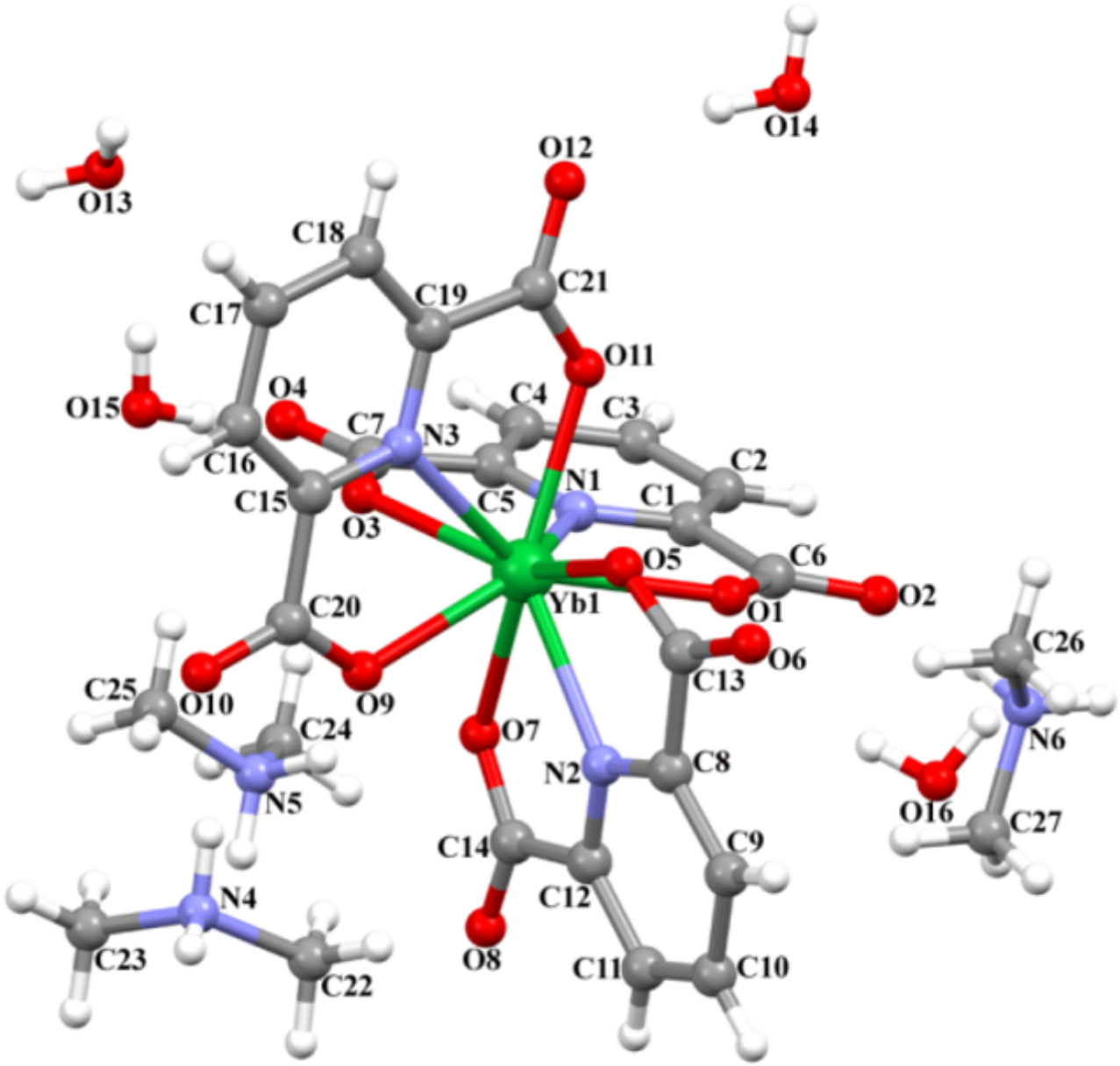

Figure 2

The molecular structure of 1 showing the atom numbering scheme

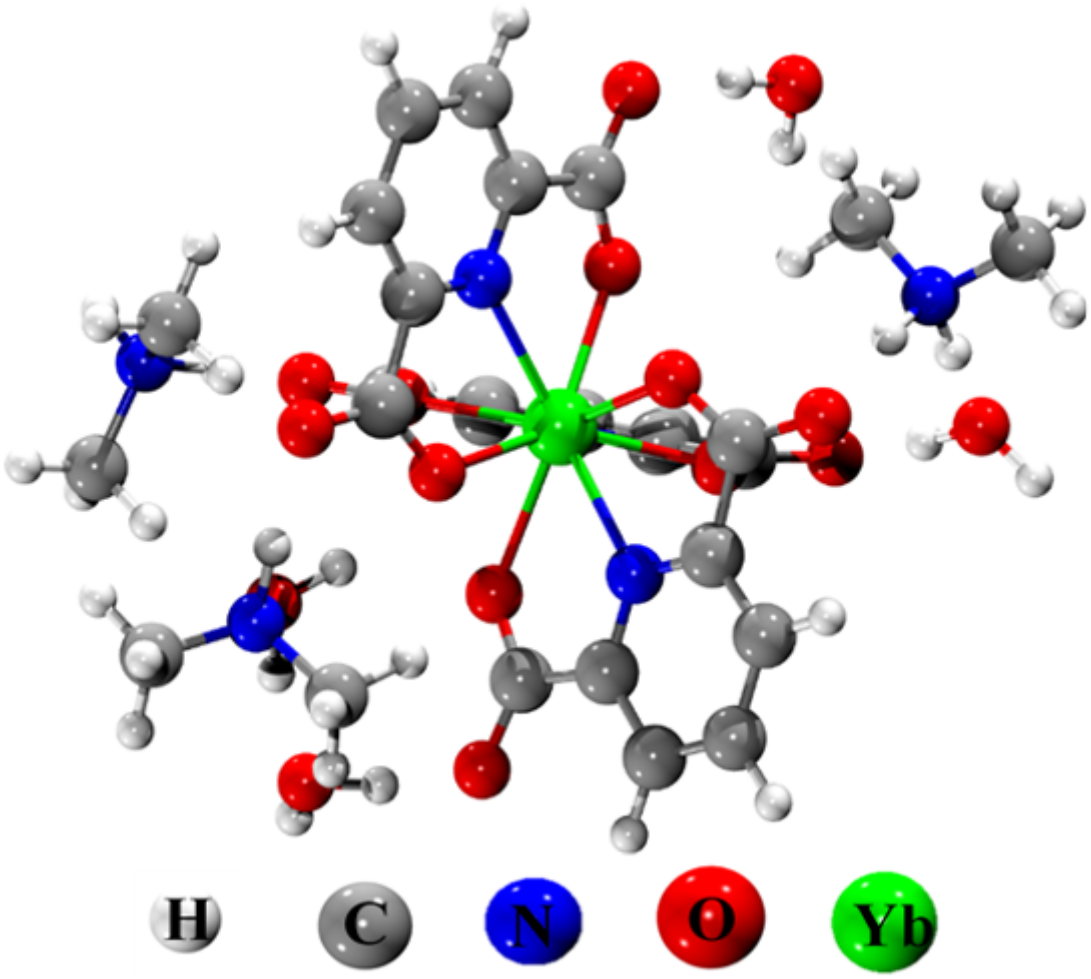

Figure 3

Optimized geometry of complex 1 at B3LYP/SDD level of theory

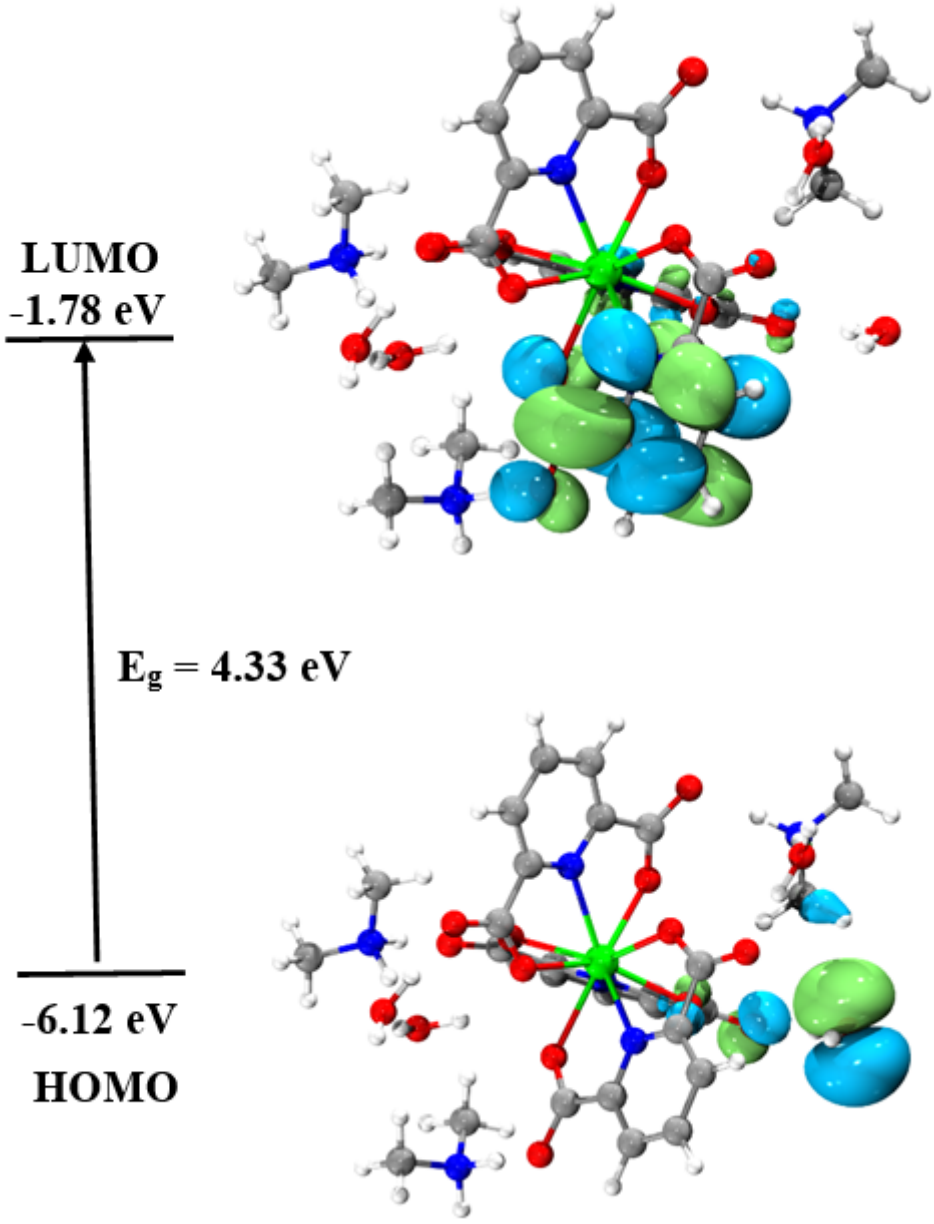

Figure 4

Surface plots of HOMO and LUMO of complex 1 and their energy gap Eg (eV)

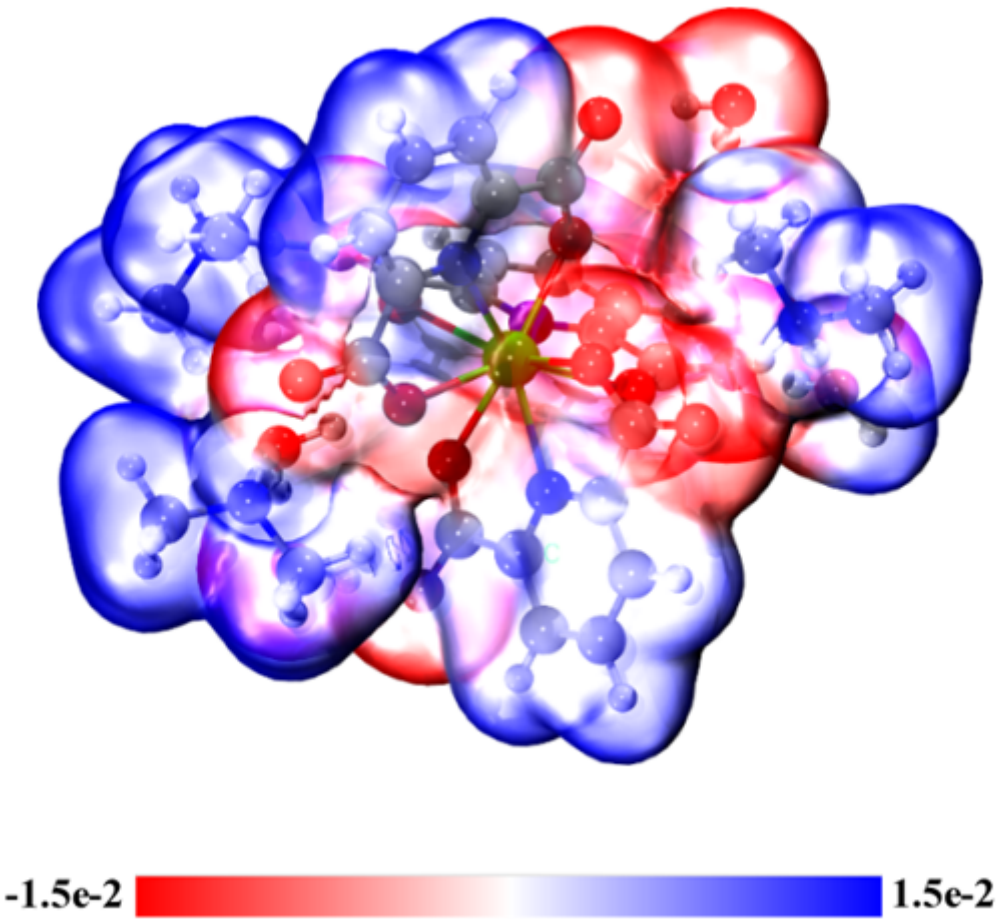

Figure 5

Molecular electrostatic potential (MEP) surface of complex 1

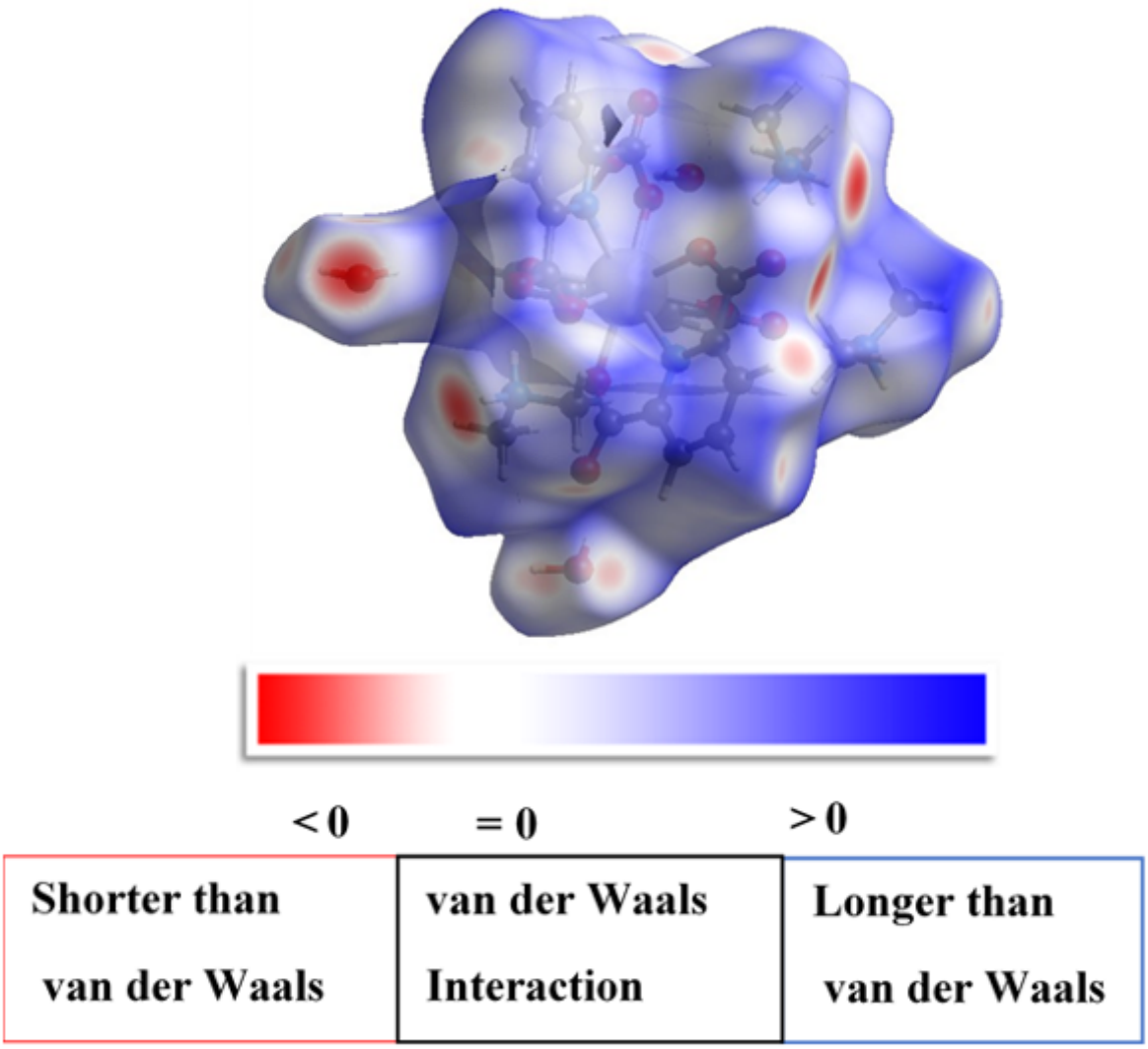

Figure 6

Hirshfeld dnorm surface map of complex 1 reflecting intermolecular interactions

Supplementary Files

This is a list of supplementary files associated with this preprint. Click to download.

- JIOPM2021Supplementarymaterial.docx
- Ybcheckcif.pdf
- YbCCDC.txt